IOPscience iopscience.iop.org

Home Search Collections Journals About Contact us My IOPscience

Path-integral approach to lattice polarons

This article has been downloaded from IOPscience. Please scroll down to see the full text article.

2007 J. Phys.: Condens. Matter 19 255213

(http://iopscience.iop.org/0953-8984/19/25/255213)

View the table of contents for this issue, or go to the journal homepage for more

Download details:
IP Address: 129.252.86.83
The article was downloaded on 28/05/2010 at 19:21

Please note that terms and conditions apply.

IOP PUBLISHING JOURNAL OF PHYSICS: CONDENSED MATTER

J. Phys.: Condens. Matter **19** (2007) 255213 (16pp) doi:10.1088/0953-8984/19/25/255213

Path-integral approach to lattice polarons

P E Kornilovitch

Hewlett-Packard, Corvallis, OR 97330, USA

E-mail: pavel.kornilovich@hp.com

Received 31 October 2006, in final form 12 January 2007
Published 30 May 2007
Online at stacks.iop.org/JPhysCM/19/255213

Abstract

The basic principles behind a path integral approach to the lattice polaron are reviewed. Analytical integration of phonons reduces the problem to one self-interacting imaginary-time path, which is then simulated by Metropolis Monte Carlo. Projection operators separate states of different symmetry, which provides access to various excited states. Shifted boundary conditions in imaginary time enable calculation of the polaron mass, spectrum and density of states. Other polaron characteristics accessible by the method include the polaron energy, number of excited phonons and isotope exponent on mass. Monte Carlo updates are formulated in continuous imaginary time on infinite lattices and as such provide statistically unbiased results without finite-size and finite time-step errors. Numerical data are presented for models with short-range and long-range electron–phonon interactions.

1. Introduction

The polaron has been a testing ground for novel theoretical methods for three-quarters of a century. Perhaps the best example is the statistical path integral (PI) that was applied to the Fröhlich polaron by Feynman in 1955 [1], just a few years after the invention of the PI. The combination of analytical integration of phonons and a variational principle proved so powerful that this approach has dominated the physics of the Fröhlich polaron for decades [2–17], and continues to do so today 50 years after the seminal paper. PI has not been utilized for a long time in the physics of small or lattice polarons. Although the phonons could be integrated as well leading to a self-interacting one-electron system, the absence of a convenient trial action rendered the variational part of the calculation intractable. The situation changed in 1982 when de Raedt and Lagendijk (DRL) noticed that the self-interaction can be instead simulated on a computer by Metropolis Monte Carlo (MC) [18–21]. This paved the way to an efficient MC algorithm that provided accurate polaron energies and static correlation functions. Later on, the DRL method was re-formulated in continuous time that removed the finite time-step systematic error [22]. Application of open boundary conditions in imaginary time enabled

 © 2007 IOP Publishing Ltd Printed in the UK

unbiased calculations of such important polaron properties as the effective mass, spectrum, density of states and the isotope exponent on mass [23–29].

Thus, the continuous-time path-integral quantum MC (PIQMC) became another theoretical tool tested on the polaron problem. It is not the only MC method available for analysis of the polaron problem. Other powerful methods developed in the last decade include the diagrammatic MC [30–32] and Lang–Firsov MC [33, 34]. All methods have their own advantages and limitations.

In this paper the main principles behind the PIQMC polaron method are reviewed. Particular attention is paid to the use of projection operators that allow access to excited states of different symmetries. Phonon integration is performed for open boundary conditions in imaginary time, which are necessary for calculating the polaron mass. A number of numerical results on the polaron properties are presented for both the short-range Holstein and long-range electron–phonon (e–ph) interactions. In particular, it is shown that a long-range e–ph interaction dramatically reduces the polaron mass, and anisotropic e–ph interaction exponentially enhances the anisotropy of the polaron spectrum.

2. Projected partition functions

A thermodynamic partition function receives contributions from all states of a many-body system. If the system possesses a global symmetry, however, the entire Hilbert space can be subdivided into sectors which correspond to different irreducible representations of the symmetry group G. Because the system remains within the sector during its evolution, it is meaningful to compose a partial partition function which runs over just one sector. Then the full partition function is simply a sum of the partial partition functions.

This idea can be translated into the language of PI. The conventional statistical PI is developed from the trace of the density matrix

$$Z = \sum_{\mathbf{R}} \langle \mathbf{R}|\mathrm{e}^{-\beta H}|\mathbf{R}\rangle = \sum_{\mathbf{R}} \int_{(\mathbf{R},0)}^{(\mathbf{R},\beta)} \mathcal{D}\mathbf{R}(\tau) W[\mathbf{R}(\tau)], \tag{1}$$

where $\mathbf{R}$ is a many-body real-space configuration, H is the Hamiltonian, $\beta = (k_\mathrm{B}T)^{-1}$, τ is the imaginary time, $0 \leqslant \tau \leqslant \beta$ and W is the statistical weight of path $\mathbf{R}(\tau)$. In contrast, a partial partition function corresponding to an irreducible representation U leads to the following PI

$$Z_U = \sum_{\mathbf{R}} \langle \mathbf{R}|O_U^\dagger \mathrm{e}^{-\beta H} O_U|\mathbf{R}\rangle = \sum_{\mathbf{R}} \sum_T O_U(T) \int_{(\mathbf{R},0)}^{(T\mathbf{R},\beta)} \mathcal{D}\mathbf{R}(\tau) W[\mathbf{R}(\tau)]. \tag{2}$$

Here T is a symmetry operator of group G, while the operator O_U creates a basis state of U from any real-space configuration $\mathbf{R}$. In this PI, the initial configuration of the path (at $\tau = 0$) and the final configuration of the path (at $\tau = \beta$) differ by a symmetry transformation T. After that, the operation $\sum_T O_U(T)$ projects the PI on the U sector of Hilbert space. For this reason the partial partition functions will hereafter be called *projected* partition functions. In the low-temperature limit $\beta \to \infty$, equation (2) provides access to the ground state of sector U, in the same manner as the conventional PI provides access to the global ground state.

There exist multiple instances when this approach yields important information about excited states of a quantum-mechanical system. For example, for a system of identical particles, G is the permutation group, T is a permutation operator P and U is a particular representation of G, defined by the corresponding Young table. Thus in a Monte Carlo process the top ends of the paths are constantly permutated with respect to the bottom ends of the paths [35]. The operator $O_S(P) = (+1)$ for the fully symmetric representation (bosons) and $O_A(P) = (-1)^{\text{parity of } P}$ for the fully antisymmetric representation (spinless fermions); there

are more complex forms for other representations. In polaron physics, this approach can be applied to separate singlet and triplet bipolarons. Analogously, by allowing 90° rotations of the top ends with respect to the bottom ones, it is possible to separate s- and d-symmetric bipolarons on the square lattice.

Another important global symmetry is translation invariance. In this case, T is the translation operator, U is labelled by the total lattice momentum $\mathbf{K}$ and $O_{\mathbf{K}}(T_{\Delta\mathbf{r}}) = \mathrm{e}^{\mathrm{i}\mathbf{K}\Delta\mathbf{r}}$, where $\Delta\mathbf{r}$ is the parallel-shift vector between the top and bottom path ends. Equation (2) then provides the ground state energy as a function of $\mathbf{K}$. For the case of one or two particles interacting with phonons, this implies the (bi)polaron spectrum $E(\mathbf{K})$, the effective mass, the density of states and their derivatives. Equation (2) becomes

$$Z_{\mathbf{K}} = \sum_{\Delta\mathbf{r}} \mathrm{e}^{\mathrm{i}\mathbf{K}\Delta\mathbf{r}} \langle \mathbf{R} + \Delta\mathbf{r} | \mathrm{e}^{-\beta H} | \mathbf{R} \rangle = \sum_{\Delta\mathbf{r}} \mathrm{e}^{\mathrm{i}\mathbf{K}\Delta\mathbf{r}} \int_{(\mathbf{R},0)}^{(\mathbf{R}+\Delta\mathbf{r},\beta)} \mathcal{D}\mathbf{R}(\tau) W[\mathbf{R}(\tau)], \tag{3}$$

where $\mathbf{R} + \Delta\mathbf{r}$ denotes 'configuration $\mathbf{R}$ parallel-shifted by $\Delta\mathbf{r}$'. A Monte Carlo process constantly updates $\Delta\mathbf{r}$ by parallel-shifting the top configuration relative to the bottom one. Then the operation $\sum_{\Delta\mathbf{r}} \exp(\mathrm{i}\mathbf{K}\Delta\mathbf{r})$ projects simulation on a particular lattice momentum $\mathbf{K}$. For a detailed derivation of (3), see [24, 36].

Once the update process has been established, the observables are obtained in the usual manner. The ground state energy of a (bi)polaron (i.e. at $\mathbf{K} = 0$) can be found as the low-temperature limit of the internal energy $E_0 = -\partial \ln Z_0/\partial\beta$. Applying this to equation (3) one obtains

$$E_0 = \frac{\sum_{\Delta\mathbf{r}} \int_{(\mathbf{R},0)}^{(\mathbf{R}+\Delta\mathbf{r},\beta)} \mathcal{D}\mathbf{R}(\tau) \left[-\frac{1}{W}\frac{\partial W}{\partial\beta} \right] W[\mathbf{R}(\tau)]}{\sum_{\Delta\mathbf{r}} \int_{(\mathbf{R},0)}^{(\mathbf{R}+\Delta\mathbf{r},\beta)} \mathcal{D}\mathbf{R}(\tau) W[\mathbf{R}(\tau)]} = \left\langle -\frac{1}{W}\frac{\partial W}{\partial\beta} \right\rangle_{\text{shift}}, \tag{4}$$

where the subscript means that averaging is performed under the shifted boundary conditions in imaginary time. A specific expression for the combination in angular brackets will be derived below. Next, by taking the ratio of $Z_{\mathbf{K}}$ and Z_0 one obtains the estimator for the (bi)polaron spectrum

$$E_{\mathbf{K}} - E_0 = -\lim_{\beta\to\infty} \frac{1}{\beta} \ln\langle \cos \mathbf{K}\Delta\mathbf{r} \rangle_{\text{shift}}. \tag{5}$$

This expression contains a sign problem: if the energy difference being calculated is significantly larger than the temperature, the mean cosine becomes exponentially small. However, when the energy difference is comparable with temperature, this estimator is stable. Note that statistics for multiple lattice momenta can be collected in a single MC run. This enables efficient calculation of the (bi)polaron density of states by histogramming energy values at the end of simulations. Expansion of the last expression for small $\mathbf{K}$ yields another important estimator, the μth component of the (bi)polaron inverse effective mass

$$\frac{1}{m^*_\mu} = \lim_{\beta\to\infty} \frac{\langle (\Delta r_\mu)^2 \rangle_{\text{shift}}}{\hbar^2\beta}. \tag{6}$$

If β is regarded as diffusion time and $\langle (\Delta r_\mu)^2 \rangle$ as a mean-squared diffusion distance then the *inverse mass is the diffusion coefficient of an open-ended imaginary path*. This relation holds for any composite particle.

3. Polaron action

The results derived in the previous section apply to any quantum-mechanical system. The specific feature of a polaron system is a strong interaction between a small number of electrons

and a large number of phonons. In the following, the consideration will be limited to a generic 'density–displacement' electron–phonon (e–ph) Hamiltonian

$$H = -t\sum_{\mathbf{nn}'} c^{\dagger}_{\mathbf{n}'}c_{\mathbf{n}} - \sum_{\mathbf{nm}} f_{\mathbf{m}}(\mathbf{n})c^{\dagger}_{\mathbf{n}'}c_{\mathbf{n}}\xi_{\mathbf{m}} + \sum_{\mathbf{m}}\left(-\frac{\hbar^2}{2M}\frac{\partial^2}{\partial\xi^2_{\mathbf{m}}} + \frac{M\omega^2}{2}\xi^2_{\mathbf{m}}\right). \tag{7}$$

The electron subsystem is represented by a single band with nearest-neighbour hopping amplitude t, and the phonon subsystem by a set of non-interacting Einstein oscillators with frequency ω and ion mass M. Both restrictions are non-critical and can be handled by the present approach [37]. Here most attention will be devoted to the middle e–ph term. The function $f_{\mathbf{m}}(\mathbf{n})$ is the *force* with which an electron at site $\mathbf{n}$ is acting on oscillator $\xi_{\mathbf{m}}$. Function f is subjected to obvious physical restrictions, but is arbitrary otherwise. In particular it can be short-range (Holstein interaction) as well as long-range (Fröhlich interaction) and anisotropic. In the atomic limit, $t = 0$, a static polaron experiences a downward energy shift of $E_{\mathrm{p}} = (2M\omega^2)^{-1}\sum_{\mathbf{m}} f^2_{\mathbf{m}}(0)$ (the *polaron shift*), which can be taken as a measure of the strength of e–ph interaction. The respective dimensionless quantity is the ratio of E_{p} and some measure of the electron kinetic energy, e.g. zt, where z is the number of nearest neighbours on the lattice:

$$\lambda = \frac{E_{\mathrm{p}}}{zt} = \frac{1}{2M\omega^2 zt}\sum_{\mathbf{m}} f^2_{\mathbf{m}}(0). \tag{8}$$

For the short-range Holstein interaction, $f_{\mathbf{m}}(\mathbf{n}) = \kappa\delta_{\mathbf{nm}}$, and $\lambda = \kappa^2/(2M\omega^2 zt)$. The second parameter of the model is the adiabaticity ratio $\bar{\omega} \equiv \hbar\omega/t$.

A key element of the PI polaron method is analytical integration of phonon variables. Following Feynman it can be done exactly [1, 38]. Phonon integration results in self- and cross-interaction of polaron paths. Because the phonons possess their own dynamics, the interactions are retarded. This means that different parts of a polaron path 'feel' each other if they are separated in imaginary time by less than inverse phonon frequency. The self-interaction increases the statistical weight of straighter paths, making them on average more rigid. That means that an open-ended path diffuses less in imaginary time, which by virtue of (6) implies an enhanced effective mass. Thus path integrals provide a useful visualization of mass increase caused by interaction with phonons.

In performing phonon integration it is important to keep in mind that the shifted boundary conditions described in the previous section refer to the full set of system degrees of freedom. Therefore the electron and ion coordinates are always correlated. If the electron path is shifted by a vector $\Delta\mathbf{r}$ between times $\tau = 0$ and β then the *entire* phonon configuration at $\tau = \beta$ must be shifted with respect to $\tau = 0$ by exactly $\Delta\mathbf{r}$ (see figure 1(a)). As a result, the boundary conditions for individual oscillators are not periodic but rather satisfy the condition $\xi_{\mathbf{m}}(\beta) = \xi_{\mathbf{m}-\Delta\mathbf{r}}(0)$. This is a subtle but important point, apparently missed by Feynman himself. These new boundary conditions make the mass calculation self-consistent—for a detailed discussion consult [36]. The full polaron action acquires a correction ΔA relative to the familiar periodic expression A_0 [22]

$$A_{\mathrm{pol}}[\mathbf{r}(\tau)] = A_0 + \Delta A, \tag{9}$$

$$A_0 = \sum_{\mathbf{m}}\frac{\hbar}{4\omega M}\int_0^{\beta}\int_0^{\beta} \mathrm{d}\,\tau\,\mathrm{d}\tau'\frac{\cosh\hbar\omega(\frac{\beta}{2} - |\tau-\tau'|)}{\sinh\hbar\omega\frac{\beta}{2}}F_{\mathbf{m}}(\tau)F_{\mathbf{m}}(\tau'), \tag{10}$$

$$\Delta A = \sum_{\mathbf{m}}\frac{\hbar}{2\omega M}B_{\mathbf{m}}(C_{\mathbf{m}+\Delta\mathbf{r}} - C_{\mathbf{m}}), \tag{11}$$

$$B_{\mathbf{m}} \equiv \int_0^{\beta}\mathrm{d}\tau'\frac{\sinh\hbar\omega(\beta-\tau')}{\sinh\hbar\omega\beta}F_{\mathbf{m}}(\tau'), \tag{12}$$

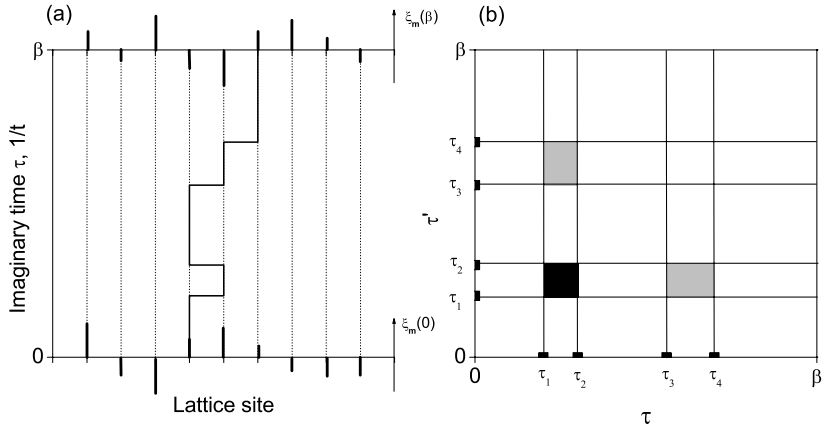

Figure 1. (a) Integration over ionic paths under shifted boundary conditions. Ionic displacements are shown as vertical bars at $\tau = 0$ and β. Note how the pattern of displacements is correlated with the shift of the electron path. The end displacements of individual oscillators are not equal, $\xi_{\mathbf{m}}(0) \neq \xi_{\mathbf{m}}(\beta)$. (b) Calculation of the polaron action as a double integral over imaginary time. The kink times τ_i breaks the $(\tau\tau')$ plane into a finite number of rectangles. Within each rectangle the electron coordinates are constant and the double integral can be calculated analytically for arbitrary τ_i [28]. After that the double integral reduces to a sum over the rectangles. Since the number of rectangles decreases at strong coupling, the algorithm gets faster at *strong* coupling.

$$C_{\mathbf{m}} \equiv \int_0^\beta \mathrm{d}\tau' \frac{\sinh \hbar\omega\tau'}{\sinh \hbar\omega\beta} F_{\mathbf{m}}(\tau'). \tag{13}$$

This action increases the weight of electron paths as $\sim\exp(A)$. The simple form of ΔA, equation (11), is valid only when the condition $\exp(\beta\hbar\omega) \gg 1$ is satisfied. The function $F_{\mathbf{m}}(\tau)$ is the force that the oscillator $\mathbf{m}$ experiences at time τ. For the one-electron (polaron) case, there is only one path $\mathbf{r}(\tau)$ which is the sole source of force, hence $F_{\mathbf{m}}(\tau) = f_{\mathbf{m}}[\mathbf{r}(\tau)]$. For the two-particle (bipolaron) case, there are two electron paths, and $F_{\mathbf{m}}(\tau) = f_{\mathbf{m}}[\mathbf{r}_1(\tau)] + f_{\mathbf{m}}[\mathbf{r}_2(\tau)]$. Since the action is quadratic in F, it breaks into four terms. The diagonal ones describe the self-interaction of the two electron paths and are responsible for the polaronic effects. The cross-terms describe the interaction between the paths and are responsible for polaron binding. This distinction naturally carries over to the multi-electron case.

In general, numerical evaluation of the double integral in the above equation constitutes a considerable technical difficulty. This task is greatly aided by the fact that on a lattice the polaron path consists of a *finite* number of straight segments (see figure 1(a)). Within segment i the electron position $\mathbf{r}_i$ is constant. Consequently, force $F(\tau)$ is constant, too, and hence can be taken outside the time integration. Then the time double integral can be calculated analytically, resulting in a simple analytical function of the segment end times $A(\tau_i, \tau_i'; \tau_j, \tau_j')$. Explicit expressions are given in [28]. The polaron action then becomes a double sum over the segments (see figure 1(b)):

$$A_{\mathrm{pol}} = \sum_{j\geqslant i} A(\tau_i, \tau_i'; \tau_j, \tau_j') \sum_{\mathbf{m}} f_{\mathbf{m}}(\mathbf{r}_i) f_{\mathbf{m}}(\mathbf{r}_j) \equiv \sum_{j\geqslant i} A(\tau_i, \tau_i'; \tau_j, \tau_j') \Phi(\mathbf{r}_i - \mathbf{r}_j), \tag{14}$$

where the *path confinement function* $\Phi(\mathbf{r} - \mathbf{r}')$ has been introduced. It is defined on a discrete set of points and can be pre-computed for a sufficiently large range of coordinate separation. After that action calculation takes essentially the same amount of time for *any* shape of the electron–phonon interaction.

4. Continuous-time Monte Carlo

On a lattice, an electron's path can be specified by a set of *kinks* that connect the sites before and after an electron's hops, and by the times at which these hops occur. Between the neighbouring kinks, the path is straight and occupies a particular lattice site. By expanding the short-time propagator $\langle \mathbf{r}' | \exp(-\Delta\tau H_{\rm kin}) | \mathbf{r} \rangle$ to the first power in $\Delta\tau$, it is a simple matter to show that each kink contributes to the path's weight by a factor $(t\,\Delta\tau)$, while each straight segment contributes a factor of 1. In the continuous time limit $\Delta\tau$ becomes infinitesimal. The partition function is a sum over all possible paths, i.e. over different kink numbers and their times. The denominator of equation (4) becomes (see also equation (3) at $\mathbf{K} = 0$)

$$Z_{\mathbf{K}=0} = Z_{\rm ph} \sum_{N_k=0,1,\ldots}^{\infty} \int_0^\beta \cdots \int_0^\beta (\mathrm{d}\tau)^{N_k} t^{N_k} \mathrm{e}^{A_{\rm pol}[\mathbf{r}(\tau)]}. \tag{15}$$

Here $Z_{\rm ph} = [2\sinh(\frac{1}{2}\hbar\beta\omega)]^{-N}$ (N is the number of lattice sites) is the partition function of free phonons. It is a multiplicative constant that cancels out from all statistical averages. $A_{\rm pol}$ is the polaron action (9). The weight of the full path combines the 'kinetic' contribution $(t d\tau)^{N_k}$ and the 'potential' contribution $\exp(A_{\rm pol})$. Note that because the two ends of a polaron path are not tied together, the number of kinks N_k on the path can be arbitrary.

The integrand of the partition function (15) can be stochastically sampled, enabling statistical averaging of observables. Updates that do not change the number of kinks on the path are defined only by the potential contribution $\exp(A_{\rm pol})$ of the configurations before and after the update. Updates that do change N_k are trickier because they change the power of the infinitesimal $(\mathrm{d}\tau)$, which renders direct comparison of the two weights impossible. These updates are organized as follows. Consider an update when a kink at time τ is added to path D. The resulting path is D'. The general detailed balance equation reads

$$W(D)Q(\text{add at } \tau)P(D \to D') = W(D')Q(\text{remove at } \tau)P(D' \to D), \tag{16}$$

where Q is the probability of proposing the update and P the probability of accepting the suggestion. According to (15), $W(D) = (t\,\mathrm{d}\tau)^{N_k} \exp\{A_{\rm pol}(D)\}$ and $W(D) = (t\,\mathrm{d}\tau)^{N_k+1} \exp\{A_{\rm pol}(D')\}$. The probabilities Q on the two sides of the balance equation are two different quantities. In the direct process, the probability of suggesting a kink in the interval $[\tau, \tau + \mathrm{d}\tau]$ is proportional to the time interval $\mathrm{d}\tau$, and can therefore be represented as $Q_{\rm add}(\tau) = q(\tau)\,\mathrm{d}\tau$, where $q(\tau)$ is the probability *density* of proposing the new kink at time τ. In contrast, in the reciprocal process of removing a kink, the probability of suggesting a particular kink from the existing N_k+1 is a *finite* number. Thus the relative smallness of $W(D')$ is compensated by an additional $(t\,\mathrm{d}\tau)$ in $Q_{\rm add}$. In the simplest update scheme, all kinks are inserted with a constant probability density $q(\tau) = \beta^{-1}$, and removed with equal probability $Q_{\rm remove} = (N_k + 1)^{-1}$. The balance equation becomes

$$(t\Delta\tau)^{N_k} \frac{1}{\beta} (\Delta\tau) \mathrm{e}^{A_{\rm pol}(D)} P(D \to D') = (t\Delta\tau)^{N_k+1} \frac{1}{N_k+1} \mathrm{e}^{A_{\rm pol}(D')} P(D' \to D). \tag{17}$$

Following the recipe of Metropolis Monte Carlo [39], this equation leads to the following acceptance rules:

$$P(D \to D') = \min\left\{1;\ \frac{\beta t}{N_k+1} \mathrm{e}^{A_{\rm pol}(D') - A_{\rm pol}(D)}\right\}, \tag{18}$$

$$P(D' \to D) = \min\left\{1;\ \frac{N_k+1}{\beta t} \mathrm{e}^{A_{\rm pol}(D) - A_{\rm pol}(D')}\right\}. \tag{19}$$

The above acceptance rules are valid for updates between configurations with non-zero kink numbers, i.e. $1 \leftrightarrow 2$, $2 \leftrightarrow 3$, ... For the transition $0 \leftrightarrow 1$, one has to take into account that

kinks can only be inserted if $N_k = 0$ while they can be inserted or removed if $N_k = 1$. This results in an additional $\frac{1}{2}$ in the acceptance rules: βt should be replaced with $\frac{1}{2}\beta t$.

Once the sampling process is established, the polaron mass and spectrum can be measured according to equations (6) and (5), respectively. The estimator for the ground state energy of the polaron follows from the general formula (4) and the path's weight $W(N_k) = (t\,\mathrm{d}\tau)^{N_k}\exp(A_{\mathrm{pol}})$:

$$E_0 = \left\langle -\frac{N_k}{\beta} - \frac{\partial A_{\mathrm{pol}}}{\partial\beta}\right\rangle_{\mathrm{shift}}. \tag{20}$$

The first term of the estimator is the kinetic energy of the polaron. (To derive it, it is convenient to momentarily return to the discrete-time representation: $\mathrm{d}\tau \to \beta/L$, where L is the number of time slices, and then to differentiate with respect to β.) Note that each kink contributes the same value of β^{-1}. The second term in (20) is the potential energy of the polaron, that is the sum of the electron–phonon energy and the energy of lattice deformation.

The number of excited phonons in the polaron cloud can be obtained by differentiating the free energy $F = -\frac{1}{\beta}\ln Z$ with respect to the phonon frequency $\hbar\omega$ while keeping the combination $\lambda/(M\omega)$ constant. This condition ensures that the derivative will affect only the free phonon part of the Hamiltonian. One obtains

$$N_{\mathrm{ph}} = -\frac{1}{\beta}\frac{\partial F}{\partial(\hbar\omega)}\bigg|_{\frac{\lambda}{M\omega}} = -\frac{1}{\beta}\left\langle\frac{\partial A_{\mathrm{pol}}}{\partial(\hbar\omega)}\bigg|_{\frac{\lambda}{M\omega}}\right\rangle_{\mathrm{shift}}. \tag{21}$$

Another interesting (bi)polaron characteristic is the isotope exponent on the effective mass. In the (bi)polaron mechanism of superconductivity, α_μ is related to the isotope effect on the critical temperature [40]. The mass isotope exponent is defined as $m^*_\mu = M^{\alpha_\mu}$, where M is the ion mass. Since the present method calculates the inverse polaron mass, α_μ is more conveniently expressed via the inverse effective mass

$$\alpha_\mu = -\frac{M}{\frac{1}{m^*_\mu}}\frac{\partial}{\partial M}\left(\frac{1}{m^*_\mu}\right) = \frac{\omega}{2\left(\frac{1}{m^*_\mu}\right)}\frac{\partial}{\partial\omega}\left(\frac{1}{m^*_\mu}\right). \tag{22}$$

The last transformation follows from the scaling $M \propto \omega^{-2}$. The estimator for α_μ is derived directly from the estimator for the inverse effective mass (6). A path's weight depends on the phonon frequency only via the polaron action $\exp(A_{\mathrm{pol}})$. (One should keep in mind that the definition of a Monte Carlo average $\langle(\Delta r_\mu)^2\rangle$ contains A_{pol} in the numerator and denominator.) Upon differentiation one obtains

$$\alpha_\mu = \frac{\omega}{2\langle(\Delta r_\mu)^2\rangle}\left[\left\langle(\Delta r_\mu)^2\frac{\partial A_{\mathrm{pol}}}{\partial\omega}\bigg|_{M\omega^2}\right\rangle - \langle(\Delta r_\mu)^2\rangle\left\langle\frac{\partial A_{\mathrm{pol}}}{\partial\omega}\bigg|_{M\omega^2}\right\rangle\right]. \tag{23}$$

In taking the frequency derivative, one should keep the combination $M\omega^2$ constant, as it is independent of the ion mass. As with the phonon action and potential energy, the estimators for the number of phonons and isotope exponent can be split into double sums over the path's segments. The expressions for the respective summands can be found in [28].

5. Polaron properties

In this section polaron properties obtained with the continuous-time path-integral Monte Carlo method are reviewed [22, 24, 27, 25, 26, 28, 29].

5.1. Mobile small polarons

A large polaron mass results from the small overlap of ionic wavefunctions before and after an electron hop. The wavefunctions are those of harmonic oscillators, and hence of the Gaussian shape. If the displacement of an ion is different before and after the hop, the wavefunction overlap is Gaussian in the displacement difference. At the same time, the polaron potential energy E_p (the sum of the electron–phonon interaction and energy of lattice deformation) is quadratic in displacement. Thus, in general, the polaron mass is exponential in the polaron energy:

$$m^* \approx m_0 \exp\left(\gamma \frac{E_\mathrm{p}}{\hbar\omega}\right), \tag{24}$$

where m_0 is the bare electron mass. The above formula is a result of the Lang–Firsov approximation [41]. The coefficient γ depends on the shape of the e–ph interaction. In the limit of large phonon frequencies

$$\gamma = 1 - \frac{\sum_{\mathbf{m}} f_{\mathbf{m}}(0) f_{\mathbf{m}}(\mathbf{a})}{\sum_{\mathbf{m}} f_{\mathbf{m}}^2(0)}, \tag{25}$$

where $\mathbf{a}$ is a nearest-neighbour vector. For a short-range e–ph interaction, such as the Holstein, $\gamma \approx 1$, which reflects the fact that the lattice deformation has to be created anew after every electron hop. In contrast, for a long-range e–ph interaction $\gamma < 1$, which leads to a significant exponential reduction of mass. Physically, the mass is reduced because a given oscillator is partially deformed even before the electron gets close to it. The additional displacement needed after the electron approaches is relatively small, which greatly increases the overlap integrals.

A particular long-range e–ph model was proposed in [25]. It is characterized by the following force function:

$$f_{\mathbf{m}}(\mathbf{n}) = \kappa a^2 \frac{(\mathbf{n}-\mathbf{m})_z}{|\mathbf{n}-\mathbf{m}|^3} = \frac{\kappa a^2 h}{[(\mathbf{n}-\mathbf{n}_\mathbf{m})^2 + h^2]^{3/2}}. \tag{26}$$

This is a z-projection of the unscreened Coulomb force between an electron $\mathbf{n}$ moving in the xy plane and ions $\mathbf{m}$ vibrating along the z direction. The plane of the ions is separated from the plane of electron motion by a distance h. A one-dimensional version of the model is illustrated in figure 2(a). The interaction strength is characterized by a force constant κ. The path confinement function Φ that corresponds to the force (26) is shown in figure 2(b). It needs to be compared with its short-range (Holstein) counterpart $\Phi_\mathrm{Hol}(\mathbf{r}_i - \mathbf{r}_j) = \kappa^2 \delta_{\mathbf{r}_i,\mathbf{r}_j}$. Since a path's statistical weight depends exponentially on Φ, in the case of long-range e–ph interaction the path diffuses *exponentially* more easily, leading to an exponentially smaller effective mass. This is how the mass reduction can be understood in terms of path integrals. This polaron type was named a 'small Fröhlich polaron' in [25].

The masses of the small Holstein polaron (SHP) and small Fröhlich polaron (SFP) calculated with PIQMC for $h = a$ are compared in figure 3(a) and (b). SFP is slightly heavier at small λ but much lighter at large λ. At large coupling, both masses gradually approach the Lang–Firsov limit (24) which are indicated by thin dashed (SHP) and solid (SFP) lines. SFP is always much closer to the Lang–Firsov behaviour than SHP. The ratio of the two masses is a non-monotonic function (see figure 3(c)). This observation was later confirmed by exact diagonalization [42] and variational [43, 44] methods. The most interesting property of SFP is exponential reduction of mass relative to SHP. This effect is independent of the dimensionality because it originates solely from the long-range nature of the e–ph interaction. The mass reduction can be very large. For example, in two dimensions at $\hbar\omega/t = 0.5$ and $\lambda = 1.2$, $m_\mathrm{SHP} \approx 220$ while m_SFP is only ≈ 9. For SFP, the parameter $\gamma = 0.387$ in $d = 1$

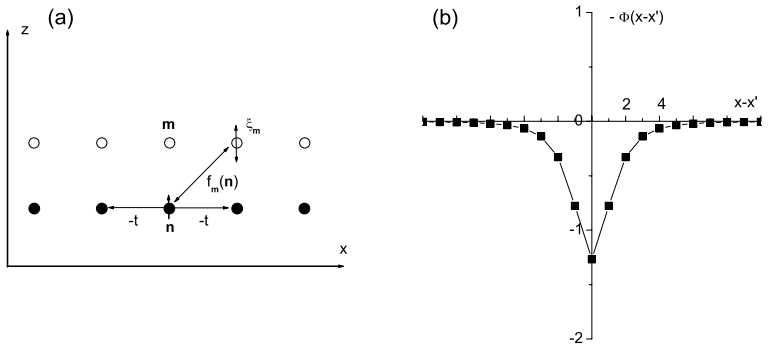

Figure 2. (a) One-dimensional model with a long-range electron–phonon interaction. The electron moves along the bottom chain of sites shown by full circles (denoted by **n**). The vibrating ions shown by open circles oscillate along the z-axis. The interaction is characterized by the z-projection of the Coulombic force (26). (b) Spatial profile of the path confinement function Φ defined in (15). The parameters are $\kappa = 1$ and $h = a$. *Negative* Φ is shown in order to draw an analogy with a potential well. This shape of Φ should be contrasted with that of the Holstein model $\Phi_{\rm Hol} = \kappa^2\delta_{xx'}$. A smooth Φ cannot localize the path as well as a sharp one, which results in a smaller effective mass in the case of a long-range model.

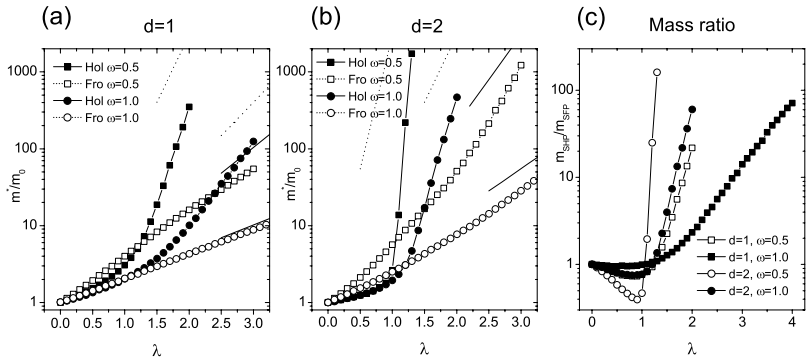

Figure 3. Effective masses of small Holstein and Fröhlich polarons in units of $m_0 = \hbar^2/(2ta^2)$: (a) $d = 1$, (b) $d = 2$. Dashed and solid thin lines indicate the strong-coupling limit $m^* = m_0 \exp(\gamma\lambda z/\bar{\omega})$ for the Holstein and Fröhlich cases, respectively. For the Holstein polaron, $\gamma = 1$. For the Fröhlich polaron, $\gamma = 0.387$ in $d = 1$ and $\gamma = 0.334$ in $d = 2$. (c) The mass ratio of the small Holstein and Fröhlich polarons for several model parameters. The ratio scales exponentially with the coupling, and could exceed 100.

and $\gamma = 0.334$ in $d = 2$. Thus the SFP mass scales roughly as the cubic root of the SHP mass. In [28], an additional screening factor was added to the force function (26). All polaron properties smoothly interpolated between those of SHP and SFP as the screening radius was changed from zero to infinity.

5.2. Anisotropy enhancement by electron–phonon interaction

In two and three dimensions an e–ph interaction can be anisotropic. In particular, it can have different effective ranges along two different lattice directions. As a result, the polaron can be heavy (Holstein-like) along one direction and at the same time much lighter (Fröhlich-like) along another direction. As functions of the e–ph strength, both masses will increase exponentially but with different parameters γ. Thus the ratio of the two masses will also be

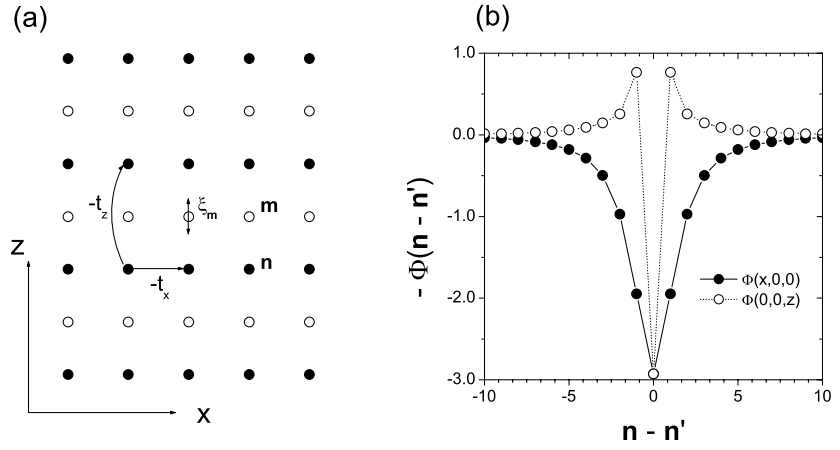

Figure 4. (a) A three-dimensional polaron model with anisotropic e–ph interaction. The electron moves within and between the planes of filled circles with hopping integrals $-t_x$ and $-t_z$, respectively. It interacts with vibrating ions shown by open circles. The vibrations are polarized along the z-axis. The distance between the planes is equal to the lattice period of the planes. In the case of a long-range interaction the polaron is Fröhlich-like in the xy plane and Holstein-like along the z direction. (b) The (negative) polaron path confinement function $-\kappa^{-2}\Phi(x, y, z)$. An additional factor $\exp(-|\mathbf{n} - \mathbf{m}|/R)$ with $R = 10$ lattice constants in the x direction has been added to the force function (26) to help the lattice sum to converge. The confining profile along z is much steeper than along x.

exponential in the polaron energy:

$$\frac{m_z}{m_x} \sim \exp\left[(\gamma_z - \gamma_x)\frac{E_\mathrm{p}}{\hbar\omega}\right]. \tag{27}$$

Therefore one should expect an *enhancement* of the anisotropy of the polaron spectrum by e–ph interaction. This effect was confirmed by exact PIQMC simulations in [26]. The model was a three-dimensional extension of (26) with the distance between the planes h being equal to the lattice period a (see figure 4(a)). For this interaction, $E_\mathrm{p} = 2.93\kappa^2/(2M\omega^2)$, and the coupling constant is defined as $\lambda = E_\mathrm{p}/(6t_x)$. Upon hopping along the z-axis, the electron must *reverse* the sign of the lattice deformation. This leads to a very small overlap of the ionic wavefunction before and after the hop. The z-effective mass is therefore even larger than in the Holstein case. In contrast, upon hopping in the xy-plane, the deformation is partially pre-existing before the hop. The overlap integrals are relatively large and the respective mass small. The difference is also reflected in the shape of the path confinement function Φ as shown in figure 4(b). It is much steeper along the z-axis than along the x-axis, which also hints at an exponential difference between the two respective masses.

The results of PIQMC analysis of the model are summarized in figure 5 [26]. Panel (a) shows a typical behaviour for the polaron masses at $\hbar\omega = 1.0t_x$ and $t_z = 0.25t_x$. (The latter choice ensures the isotropy of the bare spectrum, since the lattice constant in the z direction is twice that in the x direction.) As expected, m^*_{xy} grows exponentially with coupling. Interestingly, the z mass appears to grow *super*-exponentially with a large quadratic component: $m^*_z \approx m_{xy0}\exp(1.26\lambda + 0.88\lambda^2)$. It is possible, though, that this is still a transient regime, and m^*_z approaches pure exponential growth at still larger λ. (Even if this happens, m_z will be too large to be a physically interesting parameter.) The mass anisotropy for several sets of model parameters is shown in figure 5(b). Due to the super-exponential growth of m^*_z, the anisotropy is also super-exponential, e.g. $m^*_z/m^*_{xy} \approx \exp(0.42\lambda + 0.71\lambda^2)$ for $\hbar\omega = 1.0t_x$ (circles). At

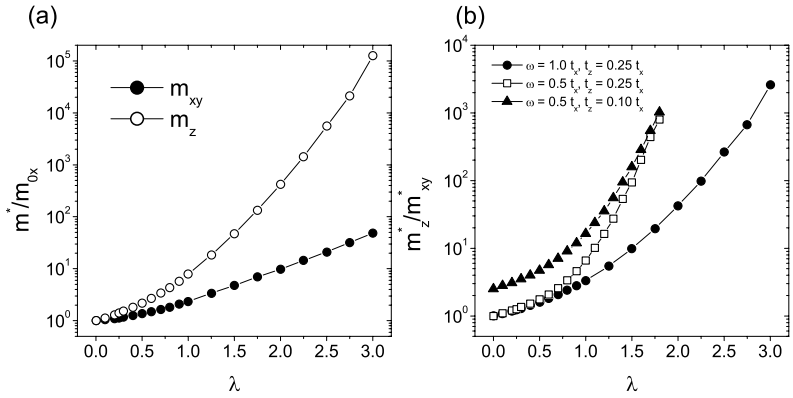

Figure 5. (a) Masses m^*_{xy} (filled circles) and m^*_z for $\hbar\omega = 1.0t_x$, $t_z = 0.25t_x$. (b) Mass anisotropy of the three-dimensional model (26) for three combinations of the model parameters. The mass anisotropy can exceed 1000.

a smaller frequency $\hbar\omega = 0.5t_x$ (squares) the anisotropy is exponentially larger, as expected from the reasoning given above. This implies the existence of an *isotope effect on the mass anisotropy*. The third model parameter, the bare hopping anisotropy, turns out to have little effect. The mass anisotropy for $t_z = 0.1\,t_x$ and the same phonon frequency $\hbar\omega = 0.5t_x$ is shown by triangles in figure 5(b). While being 2.0–2.5 times larger at small λ, the anisotropy approaches that of the $t_z = 0.25t_x$ case at large λ. This shows that it is primarily the e–ph interaction that governs the polaron anisotropy. This conclusion is further supported by studies of the Holstein model with anisotropic bare hopping [26] where *no* enhancement of the polaron anisotropy was observed.

In relation to the effect described it is interesting to note a well-documented discrepancy between the theoretical and experimental anisotropy of the cuprates [45]. According to band structure calculations, the anisotropy of resistivity of LSCO and YBCO compounds should be about 10–30 [46, 47]. At the same time, the experimental anisotropy of resistivity is between 10^2 and 10^3 depending on the level of doping. The anisotropy of bismuthates is even higher, $(5-80)\times 10^4$ [45], which is difficult to explain with the conventional Bloch–Boltzmann theory. According to the present results, anisotropic interaction with z-polarized phonons is a sufficient condition for a very large z effective mass. Of course, the anisotropy of mass and resistivity are two different things, but it would be fair to assume that the former is at least partially responsible for the latter (see, e.g., [45] page 85). This idea still awaits proper development. There are also some alternative explanations of the anomalous z-transport [48].

5.3. Peak in the polaron density of states

The estimator for the polaron spectrum is given by formula (5). There the polaron momentum $\mathbf{K}$ is simply a parameter. This means that statistics for *all* $\mathbf{K}$ can be collected during a single run. This remarkable property is a unique feature of the PIQMC method. Since the entire spectrum is calculated in one go the polaron density of states (DOS) $\rho(E) = N^{-1}\sum_{\mathbf{K}}\delta(E - E_{\mathbf{K}} + E_0)$ can be computed at the end of the run by discretizing the energy interval and histogramming $E_{\mathbf{K}}$ values.

It is well known that in the anti-adiabatic regime ($\hbar\omega \gg t$) the Holstein polaron spectrum retains its bare tight-binding shape, albeit with an exponentially reduced mass. It has been observed, however, that in the adiabatic regime ($\hbar\omega \ll t$) the polaron spectrum in $d = 1$ flattens

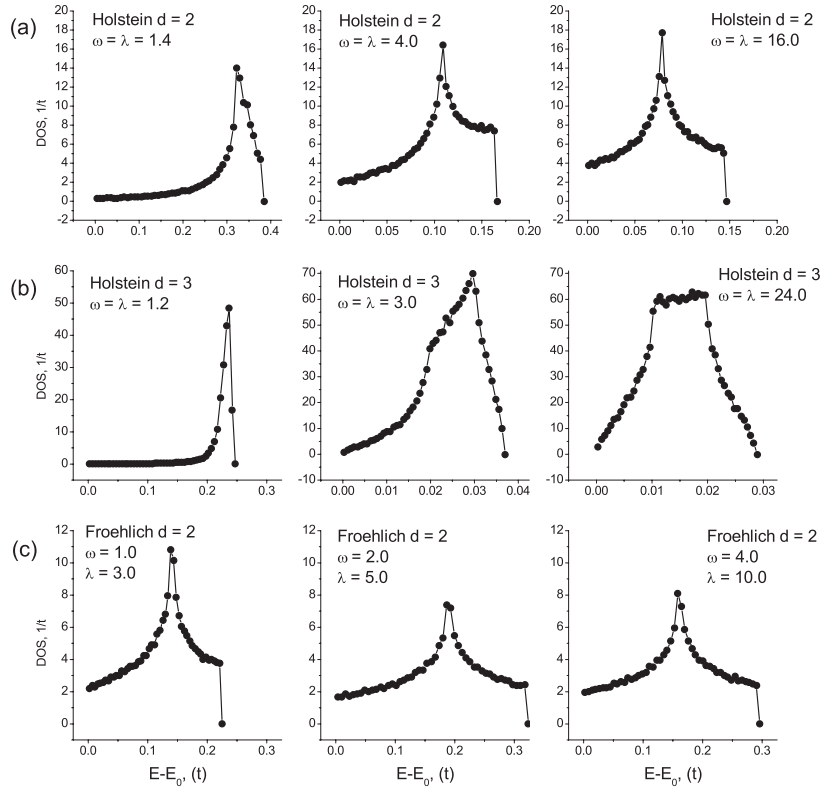

Figure 6. (a) and (b) The evolution of the density of states of the Holstein polaron with phonon frequency ω in $d = 2$ and 3, respectively. Each graph was obtained by calculating the polaron spectrum at 100 000 **K** points randomly distributed in the Brillouin zone, and histogramming the results between 50 energy bins. Each spectrum point was calculated by averaging 250 000 values of $\cos \mathbf{K}\Delta\mathbf{r}$ taken every 10th path update. Every 5000 measurements the path was reset and then equilibrated for 1000 updates. (c) The same for the small Fröhlich polaron in $d = 2$.

at large momenta [49–52]. At weak coupling the flattening can be understood as hybridization between the cosine-shaped electron spectrum and a momentum-independent phonon mode. As a result the spectrum is flatter at large **K**. At strong coupling the hybridization picture becomes less intuitive, but the flattening remains as a matter of fact. Calculation of the spectrum in higher dimensions is harder, and prior to the advent of PIQMC only a handful attempts had been made. The first full polaron spectra (i.e. over the entire Brillouin zone) and DOS in $d = 2$ and 3 were calculated in [24]. The flattening of the spectrum was found to persist. Moreover, because in high dimensions the relative weight of states with large **K** increases, the flat region of the spectrum occupies an increasingly larger volume of the Brillouin zone. As a result, DOS develops a massive peak at the top edge of the polaron band. A typical Holstein polaron DOS is shown in figures 6(a) and (b). The peak is more pronounced in $d = 3$ than in $d = 2$ because there are relatively more states with large **K**. As the phonon frequency increases DOS assumes the familiar tight-binding shapes.

The density of states of the $d = 2$ small Fröhlich polaron, characterized by the force function (26), is shown in figure 6(c). For the same total bandwidth or coupling constant this DOS is always closer to the tight-binding shape than the Holstein DOS, indicating that spectral flattening is less pronounced in long-range e–ph models. As in the effective mass case

(see figure 3) a long-range model appears to be more easily describable by the Lang–Firsov approximation than a short-range model. The observed radical transformation of the Holstein DOS suggests that care must be used in interpreting results of the short-range model in the adiabatic regime. For example, in $d = 3$ the properties of the ground state (e.g. the effective mass) have very little to do with the properties of the majority of polaron states that determine thermodynamic responses of the system.

5.4. Isotope exponents

The isotope effect is a key indicator of the importance of an e–ph interaction in a given system. The role that the isotope effect has played in the field of superconductivity is well known. In a polaron system, the e–ph interaction plays the central role. A key polaron property, the effective mass, exponentially depends on both the interaction strength and the phonon frequency (see (24)). Within the Lang–Firsov approximation the isotope exponent is (the polaron shift $E_{\rm p}$ is independent of the ion mass)

$$\alpha_{m^*} = \frac{\partial \ln m^*}{\partial \ln M} = \frac{\gamma}{2}\frac{E_{\rm p}}{\hbar\omega}. \tag{28}$$

α is proportional to the coupling constant and hence can be arbitrarily large. Therefore a large isotope exponent on mass is evidence for polaronic carriers in the system. A large isotope effect was observed, for example, on the magnetic penetration depth in cuprates [53, 54], which was interpreted as evidence for bipolaronic carriers in the superconducting state. In the weak coupling regime, α can be computed perturbatively (for the second-order results see [28, 29]). The isotope exponent is again proportional to λ but with a different coefficient. The two linear dependences should be smoothly connected over the polaron crossover.

The PIQMC method allows direct calculation of the isotope exponent as a derivative of the effective mass. The corresponding estimator is given by (23). The mass isotope exponents for the small Holstein polaron are shown in the top row of figure 7. Before the polaron transition α is small, reflecting the non-polaronic character of the carrier. Note that in $d = 2$ and 3, α is *negative* at small frequencies [29]. After the polaron crossover, which always begins at $\lambda \sim 1$ but ends at a λ that increases with ω, the isotope exponent quickly reaches the strong-coupling asymptotic behaviour (28) with $\gamma = 1$. Notice that the beginning and the end of the transition are clearly identifiable on the plots. Thus the mass isotope exponent can be useful in analysing the Holstein polaron transition.

The case of the small Fröhlich polaron is somewhat different (see the bottom row of figure 7). At small coupling, the exponent grows linearly with a γ close to the strong-coupling limit, but then deviates to smaller values. The exponent returns to the strong-coupling limit at much larger λ, the value of which decreases with increasing ω. This final approach happens when the entire path is mostly confined to one lattice site, and only rarely deviates to a first nearest neighbour. This interesting behaviour is not yet fully understood.

Apart from the isotope effect on the polaron mass, it is meaningful to consider the isotope effects on the polaron spectrum and even the density of states. Those effects have been analysed in [27].

6. Summary and path forward

We have reviewed the basics of the path-integral approach to the lattice polaron. It consists of the two main components: analytical integration of phonons and Monte Carlo simulation of a self-interacting polaron path. The phonon integration reduces the number of degrees of

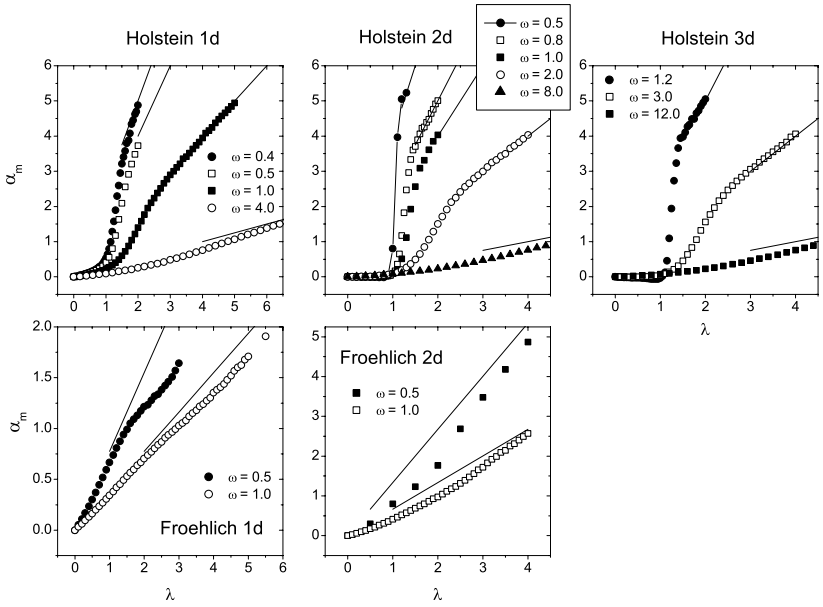

Figure 7. Mass isotope exponents of the small Holstein and small Fröhlich polarons in different dimensions and for different phonon frequencies. The thin solid lines indicate the strong-coupling limit $\alpha = \frac{\gamma}{2}\frac{\lambda z t}{\hbar\omega}$. Notice that α of the Holstein polaron in $d = 2$ and 3 is *negative* at small ω and λ.

freedom from $N + 1$ to just 1. The price for this reduction is the need to evaluate the polaron action for each polaron path. On a lattice such evaluation can be performed efficiently due to the discrete structure of the path, as described in section 3. Thus phonon integration results in a significant increase in the accuracy and efficiency of the method. Another advantage of phonon integration is the ability to treat short-range and long-range e–ph interactions on an equal footing. Precomputing the path-confining function Φ makes the time required to compute the action independent of the shape of the force function.

The power of a Monte Carlo method is the absence of any bias. The update process is approximation-free and all the estimators are statistically unbiased. As a result, all the physical properties are exact to within statistical errors. (The latter need to be dealt appropriately.) Phonon integration eliminates finite-size errors and continuous-time formulation eliminates finite time-step errors. The method works for infinite lattices of any dimensionality and symmetry.

Using this approach, several physically interesting results have been obtained. These were reviewed in the previous section. There are multiple ways in which the present algorithm can be extended beyond the single polaron with nearest neighbour hopping and dispersionless phonons. Phonon integration can be performed for any phonon dispersion and an arbitrary number of branches [37]. Long-range and anisotropic hopping can be added as long as the hopping amplitudes are negative to avoid a sign problem. Some anisotropic hopping models have already been studied in [24]. Polarons on non-cubic lattices have been analysed in [29]. Path integrals are also well suited to the study of temperature effects, which is just a parameter of the simulations. So far, no temperature effects have been analysed with this method. Perhaps the most interesting extension is beyond the single particle. The ground state of a two-polaron system, the bipolaron, is symmetric with respect to particle exchange. Therefore it can be simulated without a sign problem. Then the singlet–triplet splitting and the properties of

both bipolaron types can be calculated as explained in section 2. The first results obtained with this method have been published recently in [55–57]. Generalization to three and more particles is less straightforward because it necessarily generates a sign problem. It should be expected, however, that the fermionic sign problem will be less severe for e–ph models than for electron correlation models, such as the Hubbard model. Real-space pairing induced by phonons increases the statistical weight of even permutations over odd ones, effectively making the system more boson-like. This effect would be especially pronounced at strong e–ph couplings and low particle densities. Coupled with the capability to vary the temperature this should make it possible to calculate the critical temperature of a (bi)polaronic superconductor using the method of [58].

Acknowledgments

I would like to thank Sasha Alexandrov for long-standing collaboration and motivation for this research. I also thank James Hague and John Samson for numerous discussions on the subject of the paper. This work has been supported by the Hewlett-Packard Corporation, the EPSRC (UK), grant EP/C518365/1, and the European Science Foundation.

References

[1] Feynman R P 1955 *Phys. Rev.* **97** 660
[2] Ōsaka Y 1959 *Prog. Theor. Phys.* **22** 437
[3] Abe R and Okamoto K 1971 *J. Phys. Soc. Japan* **31** 1337
[4] Abe R and Okamoto K 1972 *J. Phys. Soc. Japan* **33** 343
[5] Saitoh M 1980 *J. Phys. Soc. Japan* **49** 878
[6] Fedyanin V K and Rodriguez C 1982 *Physica* A **112** 615
[7] De Filippis G, Cataudella V, Marigliano Ramaglia V, Perroni C A and Bercioux D 2003 *Eur. Phys. J.* B **36** 65
[8] Feynman R P, Hellwarth R W, Iddings C K and Platzman P M 1962 *Phys. Rev.* **127** 1004
[9] Thornber K K and Feynman R P 1970 *Phys. Rev.* B **1** 4099
[10] Peeters F M and Devreese J T 1984 Theory of polaron mobility *Solid State Physics* vol 38, ed F Seitz and D Turnbull (New York: Academic) pp 81–133
[11] Peeters F M and Devreese J T 1982 *Phys. Rev.* B **25** 7281
[12] Devreese J T and Brosens F 1992 *Phys. Rev.* B **45** 6459
[13] Verbist G, Peeters F M and Devreese J T 1990 *Solid State Commun.* **76** 1005
[14] Verbist G, Peeters F M and Devreese J T 1991 *Phys. Rev.* B **43** 2712
[15] Alexandrou C, Fleischer W and Rosenfelder R 1990 *Phys. Rev. Lett.* **65** 2615
[16] Alexandrou C and Rosenfelder R 1992 *Phys. Rep.* **215** 1
[17] Brosens F, Klimin S N and Devreese J T 2005 *Phys. Rev.* B **71** 214301
[18] de Raedt H and Lagendijk A 1982 *Phys. Rev. Lett.* **49** 1522
[19] de Raedt H and Lagendijk A 1983 *Phys. Rev.* B **27** 6097
[20] de Raedt H and Lagendijk A 1984 *Phys. Rev.* B **30** 1671
[21] de Raedt H and Lagendijk A 1985 *Phys. Rep.* **127** 234
[22] Kornilovitch P E 1998 *Phys. Rev. Lett.* **81** 5382
[23] Kornilovitch P E and Pike E R 1997 *Phys. Rev.* B **55** 8634
Kornilovitch P E and Pike E R 2004 *Phys. Rev.* B **69** 059902
[24] Kornilovitch P E 1999 *Phys. Rev.* B **60** 3237
[25] Alexandrov A S and Kornilovitch P E 1999 *Phys. Rev. Lett.* **82** 807
[26] Kornilovitch P E 1999 *Phys. Rev.* B **59** 13531
[27] Kornilovitch P E and Alexandrov A S 2004 *Phys. Rev.* B **70** 224511
[28] Spencer P E, Samson J H, Kornilovitch P E and Alexandrov A S 2005 *Phys. Rev.* B **71** 184310
[29] Hague J P, Kornilovitch P E, Alexandrov A S and Samson J H 2006 *Phys. Rev.* B **73** 054303
[30] Prokof'ev N V and Svistunov B V 1998 *Phys. Rev. Lett.* **81** 2514
[31] Mishchenko A S, Prokof'ev N V, Sakamoto A and Svistunov B V 2000 *Phys. Rev.* B **62** 6317
[32] Macridin A, Sawatzky G A and Jarrell M 2004 *Phys. Rev.* B **69** 245111

[33] Hohenadler M, Evertz H G and von der Linden W 2004 *Phys. Rev.* B **69** 024301
[34] Hohenadler M and von der Linden W 2005 *Phys. Rev.* B **71** 184309
[35] Ceperley D M 1995 *Rev. Mod. Phys.* **67** 279
[36] Kornilovitch P E 2005 *Phys. Rev.* B **71** 094301
[37] Kornilovitch P E 2006 *Phys. Rev.* B **73** 094305
[38] Feynman R P 1972 *Statistical Mechanics* (Reading, MA: Benjamin) chapter 3, pp 78–84
[39] Metropolis N, Rosenbluth A W, Rosenbluth M N, Teller A H and Teller E 1953 *J. Chem. Phys.* **21** 1987
[40] Alexandrov A S 1992 *Phys. Rev.* B **46** 14932
[41] Lang I G and Firsov Yu A 1962 *Zh. Eksp. Teor. Fiz.* **43** 1843
Lang I G and Firsov Yu A 1963 *Sov. Phys.—JETP* **16** 1301 (Engl. Transl.)
[42] Fehske H, Loos J and Wellein G 2000 *Phys. Rev.* B **61** 8016
[43] Bonča J and Trugman S A 2001 *Phys. Rev.* B **64** 094507
[44] Perroni C A, Cataudella V and De Filippis G 2004 *J. Phys.: Condens. Matter* **16** 1593
[45] Cooper S L and Gray K E 1994 Anisotropy and interlayer coupling in the high-T_c cuprates *Physical Properties of High-Temperature Superconductors* vol IV, ed D M Ginsberg (Singapore: World Scientific) pp 61–188
[46] Allen P B, Pickett W E and Krakauer H 1997 *Phys. Rev.* B **36** 3926
[47] Pickett W E 1989 *Rev. Mod. Phys.* **61** 433
[48] Alexandrov A S, Kabanov V V and Mott N F 1996 *Phys. Rev. Lett.* **77** 4796
[49] Stephan W 1996 *Phys. Rev.* B **54** 8981
[50] Wellein G, Röder H and Fehske H 1996 *Phys. Rev.* B **53** 9666
[51] Wellein G and Fehske H 1997 *Phys. Rev.* B **56** 4513
[52] Romero A H, Brown D W and Lindenberg K 1998 *J. Chem. Phys.* **109** 6540
[53] Zhao G, Hunt M B, Keller H and Müller K A 1997 *Nature* **385** 236
[54] Khasanov R, Eshchenko D G, Luetkens H, Morenzoni E, Prokscha T, Suter A, Garifianov N, Mali M, Roos J, Conder K and Keller H 2004 *Phys. Rev. Lett.* **92** 057602
[55] Hague J P, Kornilovitch P E, Samson J H and Alexandrov A S 2007 Superlight small bipolarons in the presence of strong Coulomb repulsion *Phys. Rev. Lett.* **98** 037002 (*Preprint* cond-mat/0606036)
[56] Hague J P, Kornilovitch P E, Alexandrov A S and Samson J H 2007 Unconventional pairing and bipolaronic theories *Physica* C at press
(Hague J P, Kornilovitch P E, Alexandrov A S and Samson J H 2006 *Preprint* cond-mat/0606719)
[57] Hague J P, Kornilovitch P E, Samson J H and Alexandrov A S 2007 Superlight small bipolarons *J. Phys.: Condens. Matter* **19** 255214
[58] Scalapino D J, White S R and Zhang S 1993 *Phys. Rev.* B **47** 7995